PHYSICAL REVIEW A VOLUME 57, NUMBER 5 MAY 1998

Squeezed light in a frontal-phase-modulated signal-recycled interferometer

Vijay Chickarmane and S. V. Dhurandhar
Inter University Centre for Astronomy and Astrophysics, Postbag 4, Ganeshkind, Pune 411007, India

T. C. Ralph, M. Gray, H-A. Bachor, and D. E. McClelland
Department of Physics, Faculty of Science, Australian National University, Canberra 0200, Australian Capital Territory, Australia

(Received 20 June 1997)

The application of squeezed light to a frontal-phase-modulated signal-recycled interferometer is considered. We present a simple model to understand the required spectrum of squeezing so as to make the interferometer more sensitive. In particular we analyze the broad- and narrow-band cases for signal recycling and find that the sensitivity of the detector can be enhanced provided an appropriate input squeezed spectrum is used. We also discuss the effect of using squeezed light on the bandwidth of the detector. [S1050-2947(98)01405-X]

PACS number(s): 42.50.Dv, 07.60.Ly

I. INTRODUCTION

The detection of gravitational waves is a very exciting experimental endeavor. Gravitational waves will yield new information about many astrophysical sources including compact binary systems, black hole collisions, and supernovae. However, because of the very weak interaction of gravitational waves with matter, the effects of a passing wave will be very small and hence considerable effort is going into the design of very sensitive detectors [1].

A gravitational wave of suitable polarization would bring about an effective change in the path length of light in the arms of a Michelson interferometer, which can be subsequently detected by monitoring the output intensity [1,2]. The intensity change is proportional to the gravitational wave amplitude, which is on the order of 10^{-21} over a frequency band of 10–1000 Hz. Such weak signals will be masked by many sources of noise both technical (classical laser noise, refractive index fluctuations, seismic vibrations, etc.) and fundamental (shot noise, quantum radiation pressure noise, thermal noise) in origin.

In this paper we are interested in noise associated with the light field. At low frequencies (in the gravitational wave source band), even the most highly stabilized lasers will exhibit excess intensity and frequency noise. An ideal interferometer, operating at a perfect dark fringe, will be immune to laser noise. However, in practice, the dark fringe is not perfect and in some control methods, a deliberate path-length mismatch is required. To avoid the classical laser noise, phase modulation techniques are used to effectively shift the signal to high Fourier frequencies at which the laser is shot noise limited. Three main modulation techniques have been proposed and investigated in the literature: internal modulation in which phase modulation is imposed inside the interferometer, frontal (or in-line) modulation in which phase modulation is imposed on the input beam, and external modulation in which a fraction of the input beam is picked off, modulated, and then recombined on a beam splitter with the field leaving the interferometer [3–5]. The photon noise is due to the quantum fluctuations of the detected field. It is inversely proportional to the square root of the laser power. When considered with radiation pressure error, which varies proportionally with the square root of the laser power, it can be shown [6] that, at an optimum power, the Heisenberg position or momentum minimum uncertainty limit is reached. For the proposed large-scale interferometers, the radiation pressure error is negligible compared with thermal noise and photon noise and will be ignored for the rest of this discussion. An interferometer limited by photon noise is referred to as a shot-noise-limited instrument. Under such conditions the sensitivity of the interferometer can be improved by either enhancing the signal response or reducing the photon noise.

Light-recycling techniques such as power recycling [7] and signal recycling [8] are two such methods of increasing the signal response. The photon noise can be reduced by injecting a squeezed vacuum into the unused output beam splitter port [6]. It is therefore of interest to combine both of these techniques. Earlier, it was shown that squeezed light can be used in a power recycled [9] interferometer to increase the sensitivity. In [10], a dual recycled interferometer with arm cavities, into which single-mode squeezed light is injected through the output port, was considered. The output photon number fluctuation was computed and compared to the photon number change due to the gravitational wave. However, it was assumed that the output photon number fluctuation calculated near dc was identical to the fluctuations at all other frequencies. Hence, the main result that was obtained there was that the sensitivity increases at all frequencies due to the squeezed light, without a change in the bandwidth. (The bandwidth refers to the frequency spread of the signal-to-noise ratio as calculated in Secs. II and III.) This as we will see turns out to be a particular case of how the sensitivity can be improved by a choice of the input squeezed spectrum. In general, however, the bandwidth will be modified by the squeezed input. Here we will extend the analysis to include a phase modulation scheme and determine whether squeezing can be effectively applied to these more realistic dual recycled instruments.

The use of squeezed light in an internally modulated Michelson interferometer was investigated in [11]. There the authors determined the nature of the squeezed light that must be injected. They also considered the main effects of losses and imperfect fringe visibility. In the current study we will

again consider a simple Michelson interferometer, now employing a frontal phase modulation scheme. More importantly, we use a linearized theory for treating quantum noise [12]. This technique brings out the origin of the different contributions to the noise spectra (such as the laser, the squeezed field, and the noise associated with the losses in the interferometer) and their relative contributions to the total noise. This increased insight allows us to optimize the instruments.

We then extend the study by considering a signal recycled interferometer that uses frontal phase modulation [5] into which a squeezed vacuum is injected through the signal recycling mirror. The signal recycling cavity can be tuned to increase the strength of the signal at a particular frequency. However, as the squeezing reflects off this cavity into the photo detection system, tuning the cavity alters the orientation of the reflected squeezed light and hence the requirements on the orientation of the injected squeezing. The phase modulation imposes requirements on the frequency spectrum of the squeezed light that must be injected.

In Sec. II we work out the signal-to-noise ratio (SNR) for a simple Michelson interferometer. Here the different sources of noise will be introduced. The total intensity noise spectra will be analyzed in detail and the relative importance of the various sources of noise will be discussed. The effects of imperfect fringe visibility will be commented on. In Sec. III a signal recycled interferometer will be considered and both the broad-band and the narrow-band cases will be discussed. We work out the requirements of the squeezed light that must be sent into the interferometer to increase its sensitivity. The bandwidth of the interferometer is analyzed and the effects of squeezing on it are determined. We present our conclusions in Sec. IV.

II. FRONTAL-PHASE MODULATION IN A SIMPLE MICHELSON INTERFEROMETER

Phase-modulation techniques are an effective way in which practical imperfections of the laser are avoided [13]. In the frontal-phase-modulation technique, a phase modulator (oscillating at ω_m) is placed between the laser (at frequency ω_L) and the input port of the interferometer. The modulation sidebands ($\omega_L \pm \omega_m$) go through the interferometer to be ejected towards the photodiode at the output port. The signal due to a gravitational wave at a frequency ω_s is encoded as a modulation of the carrier (which is the laser light), which produces two signal sidebands that are offset from the laser frequency (ω_L) by ω_s. These sidebands then beat with the modulation sidebands to give time varying intensities at the frequencies $\omega_m \pm \omega_s$. If the output light is processed through a spectrum analyzer then we would observe two peaks around the modulation frequency separated by twice the frequency of the gravitational wave. At such high frequencies the laser is usually quantum noise limited (QNL) and thus the detection is relatively more accurate. Consider a simple Michelson interferometer as shown in Fig. 1 [ignoring for the moment the signal recycling mirror (SRM)]. The action of the phase modulator on the ingoing laser field $E_0 e^{-i\omega_L t}$ is described as follows:

$$E_L(t) = E_0 e^{-i\omega_L t} e^{i\epsilon \sin \omega_m t}. \tag{1}$$

For a small modulation index, $\epsilon \ll 1$, we can expand the exponential to give

$$E_L(t) = E_0 \left[\left(1 - \frac{\epsilon^2}{4} \right) e^{-i\omega_L t} + \frac{\epsilon}{2} e^{-i(\omega_L - \omega_m)t} - \frac{\epsilon}{2} e^{-i(\omega_L + \omega_m)t} + (\text{H.O.S.}) \right], \tag{2}$$

where H.O.S. stands for higher-order sidebands. These sidebands are at the frequencies $\omega_L \pm 2\omega_m$, $\omega_L \pm 3\omega_m$, and so forth. They come with progressively smaller amplitudes in ϵ, which we are assuming to be much smaller than unity. We can therefore ignore these sidebands and thus, the fields that enter the interferometer are at the frequencies ω_L, $\omega_L \pm \omega_m$. Each of these fields propogate along the arms of the interferometer and after reflecting off the end mirrors, impinge on the photodiode. The interferometer is made to operate at the dark fringe for the carrier to give maximum sensitivity. The signal at the photodiode will be obtained by beating the modulation sidebands with the gravitational-wave-induced sidebands. The strength of this signal is therefore proportional to the power in the modulation sidebands. This output power in the modulation sidebands is maximized by allowing for a difference in length between the two arms Δl such that the interferometer while still being at a dark fringe for the frequency ω_L is now also at a bright fringe for $\omega_L \pm \omega_m$. The output power is related to the phase difference between the two arms by $P = P_0 \sin^2 \delta$. Since the phase difference, $\delta = \omega \Delta l / c$, this therefore implies that the length difference must be so adjusted such that $\sin(\omega_L \Delta l / c) = 0$ and $\sin(\omega_m \Delta l / c) = 1$.

We have so far described the mean fields that propogate in the interferometer. These fields are also accompanied by fluctuations. The fluctuations are described by the ''semiclassical linear input-output theory'' of quantum noise [12]. The mean fields serve as strong local oscillators against which the fluctuations beat, to give rise to the intensity noise. The electric field $E(t)$ is in general described by its mean value E_0, accompanied by its fluctuations $\delta e(t)$,

$$E(t) = [E_0 + \delta e(t)] e^{-i\omega_L t}, \tag{3}$$

where E_0 is taken to be real and is the mean of the electric field and $\delta e(t)$ represents the quantum fluctuations about this mean. Since the envelope rotates at the optical frequency, we can go into a rotating frame, in which we will consider the fluctuations in frequency space around the optical frequency. The noise can be divided into the two quadratures as is usually defined by

$$X_A = (\delta e + \delta e^\dagger),$$
$$X_P = i(\delta e^\dagger - \delta e), \tag{4}$$

where the subscript A stands for amplitude and P stands for phase. If we evaluate the intensity noise of the field [keeping terms to first order in $\delta e(t)$],

$$\langle \delta I(t)\rangle = \langle E_0^{\dagger}\delta e(t) + E_0 \delta e^{\dagger}(t)\rangle, \tag{5}$$

then in frequency space the noise variance is

$$\langle |\delta I(\omega)|^2\rangle = E_0{}^2 |X_A(\omega)|^2, \tag{6}$$

where $|X_A(\omega)|^2$ is the amplitude spectrum of the field fluctuations. We choose the normalization for the electric fields such that, E_0^2 is measured in photons/s, and for a coherent source $|X_A(\omega)|^2 = |X_P(\omega)|^2 = 1$, which defines the shot noise level. For a squeezed state either the amplitude $[|X_A(\omega)|^2]$ or the phase $[|X_P(\omega)|^2]$ noise must dip below the shot noise, still preserving the minimum uncertainty product. The amplitude and phase noise are in general frequency dependent and can also be correlated. The latter corresponds to an arbitrary alignment of the noise ellipse (at some frequency), in the X_A-X_P plane. This gives rise to the correlations described by the spectrum, $|X_{AP}(\omega)|^2$. In general the noise spectra satisfy the uncertainty product, $|X_A(\omega)|^2|X_P(\omega)|^2 - |X_{AP}(\omega)|^4 \geqslant 1$.

The various fields that enter the interferometer have been shown in Fig. 1. We assume that there will be losses in the interferometer that we simulate by allowing the end mirrors to be slightly transmitting. This has the effect of allowing some of the light propagating in the arms to be lost as well as introducing extra noise through the vacuum fluctuations which enter the interferometer. We represent these vacuum fluctuations due to the losses in the two arms by $\delta e_{v1}, \delta e_{v2}$, where the subscripts 1 and 2 mean that uncorrelated noise enters each of the two arms. We will deal with equal losses in the two arms, which implies that the reflectivities of the end mirrors are equal, $r_1 = r_2 = r$. This implies that the power loss in the arms is by a factor of $1 - r^2$. Later in this section we will comment on the case when we have imperfect fringe visibility for which $r_1 \neq r_2$. The squeezed light that enters into the output port of the interferometer is represented by δe_s. The laser fluctuations are labeled by δe_L.

Consider a gravitational wave of frequency ω_s, which is incident on the interferometer. A gravitational wave has the effect of modulating the arm lengths in antiphase. Let the phase due to the gravitational wave be $\delta\phi(t) = \phi_0 \sin \omega_s t$ in the arm along the x axis then the phase acquired along the y axis is $\delta\phi(t) = -\phi_0 \sin \omega_s t$, where ϕ_0 contains information about the gravitational wave amplitude. In terms of the gravitational wave strain h_0, $\phi_0 = (h_0 \omega_l / \omega_s) \sin \omega_s \tau/2$ [2], where τ is the round trip travel time in the interferometer arms. For signal frequencies $\omega_s \sim 1$ kHz, $\phi_0 \simeq h_0 \omega_l \tau/2$. Referring to Fig. 1, following the electric fields along one round trip of the interferometer we can set up the following equation for the output field $E_b(t)$,

$$\begin{aligned} E_b(t) = {} & \frac{r}{2}[(E_L(t-\tau_1)e^{i\delta\phi(t-\tau_1/2)} - E_L(t-\tau_2)e^{-i\delta\phi(t-\tau_2/2)}] \\ & + \frac{r}{2}[\delta e_L(t-\tau_1) - \delta e_L(t-\tau_2)] + \frac{r}{2}[\delta e_s(t-\tau_1) \\ & + \delta e_s(t-\tau_2)] + \frac{t}{\sqrt{2}}[\delta e_{v1}(t-\tau_1/2) \\ & + \delta e_{v2}(t-\tau_2/2)], \end{aligned} \tag{7}$$

where $E_L(t)$ is the laser field given by Eq. (2), τ_1 and τ_2 are the round trip travel times for light in the two arms and r, t are the reflection and transmission coefficients of the two end mirrors. We can now evaluate the output fields due to the carrier and modulation sidebands, due to the gravitational wave, the laser noise, the noise due to the losses in the arms and the reflected squeezed noise, all in parts.

We first consider the signal due to the gravitational wave and the modulation sidebands. We are therefore solving for the mean value of the total output field and therefore the fluctuating fields δe can be neglected. Since the gravitational wave is assumed to be very weak, $\phi_0 \ll 1$, we can expand the exponential $e^{\pm i\delta\phi(t)}$, in the above equation to give

$$\begin{aligned} E_{b(\mathrm{sig+mod})}(t) = {} & \frac{r}{2}\{E_L(t-\tau_1)[1 + i\,\delta\phi(t-\tau_1/2)] \\ & - E_L(t-\tau_2)[1 - i\,\delta\phi(t-\tau_2/2)]\}, \end{aligned} \tag{8}$$

where $E_{b(\mathrm{sig+mod})}(t)$ refers to the output field which contains the signal and modulation sidebands. Using Eq. (2) for $E_L(t)$, the above equation reads as

$$\begin{aligned} E_{b(\mathrm{sig+mod})}(t) = {} & \frac{r}{2}\Bigg(E_0 e^{i\omega_L \tau_1}\Bigg[(1-\epsilon^2/4) + \frac{\epsilon}{2}e^{i\omega_m(t-\tau_1)} \\ & - \frac{\epsilon}{2}e^{-i\omega_m(t-\tau_1)}\Bigg]\Bigg)[1 + i\,\delta\phi(t-\tau_1/2)] \\ & - \Bigg(E_0 e^{i\omega_L \tau_2}\Bigg[(1-\epsilon^2/4) + \frac{\epsilon}{2}e^{i\omega_m(t-\tau_2)} \\ & - \frac{\epsilon}{2}e^{-i\omega_m(t-\tau_2)}\Bigg]\Bigg)[1 - i\,\delta\phi(t-\tau_2/2)]. \end{aligned} \tag{9}$$

In writing down this equation, it is understood that we are in a frame rotating at ω_L. Since the operating point is at the dark fringe for the carrier, we can assume that the phase factors, $e^{i\omega_L\tau_1} = e^{i\omega_L\tau_2} = 1$. This implies from the above equation that the carrier (the field at ω_L) disappears. This will not be true once we deal with an interferometer with imperfect fringe visibility. Keeping terms to first order in $\delta\phi(t)$ and neglecting the terms that oscillate at $\omega_m \pm \omega_s$,[1] we get

[1]These terms, which arise due to the fact that the gravitational wave phase modulates the modulation sidebands, oscillate at $\omega_L \pm \omega_m \pm \omega_s$. They arise at the order $\phi_0 \epsilon$ and they must beat with the carrier (at ω_L) to contribute to the signal spectrum at $\omega_m \pm \omega_s$. However, since we assume that the operating point is at the dark fringe, this term will not make a contribution to the signal spectrum.

$$E_{b(\mathrm{sig+mod})}=rE_0(1-\epsilon^2/4)i\phi_0[\sin\,\omega_s(t-\tau_1/2)+\sin\,\omega_s(t-\tau_2/2)]+rE_0(\epsilon/4)e^{i\omega_m t}e^{-i\omega_m\tau}\left(-2i\,\sin\frac{\omega_m\Delta\tau}{2}\right)$$
$$-rE_0(\epsilon/4)e^{-i\omega_m t}e^{i\omega_m\tau}\left(2i\,\sin\frac{\omega_m\Delta\tau}{2}\right). \tag{10}$$

The first term in the above equation gives us the strength of the gravitational-wave-induced sidebands at the frequencies, $\omega_L\pm\omega_s$ and the second and third terms, the modulation sidebands at the frequencies $\omega_L\mp\omega_m$. Hence,

$$E_{b\mathrm{sig}}(\omega_L\pm\omega_s)=\mp\frac{r}{2}E_0(1-\epsilon^2/4)\,\phi_0 e^{\pm i\omega_s\tau/2}\cos\frac{\omega_s\Delta\tau}{4}, \tag{11}$$

$$E_{b\mathrm{mod}}(\omega_L\pm\omega_m)=-i\frac{r}{2}\epsilon E_0\,\sin\frac{\omega_m\Delta\tau}{2}e^{\pm i\omega_m\tau}$$
$$=-i\frac{r}{2}\epsilon E_0 e^{\pm i\omega_m\tau}, \tag{12}$$

where $\Delta\tau$ and τ are the difference and average, respectively, in the round trip travel time in the two arms. In Eq. (12), we have assumed that the interferometer is operated such that it is at a bright fringe for the modulation sidebands and hence $\sin\omega_m\Delta\tau/2=1$. At the photodetector the gravitational-wave-induced sidebands and the modulation sidebands beat with each other to give rise to a photocurrent oscillating at $\omega_m\pm\omega_s$. This change in the intensity is analyzed by processing the output intensity through a spectrum analyzer. We will be interested in obtaining the SNR for frequencies around the modulation frequency ω_m. The signal spectrum at $\omega_m+\omega_s$ is

$$|\delta\tilde{I}_{\mathrm{signal}}(\omega_m+\omega_s)|^2=|E_{b\mathrm{sig}}(\omega_L+\omega_s)E^*_{b\mathrm{mod}}(\omega_L-\omega_m)$$
$$+E_{b\mathrm{mod}}(\omega_L+\omega_m)E^*_{b\mathrm{sig}}(\omega_L-\omega_s)|^2$$
$$=\frac{{E_0}^4\epsilon^2r^4(1-\epsilon^2/4)^2{\phi_0}^2\,\cos^2\omega_s\Delta\tau/4}{4}. \tag{13}$$

Having worked out the signal spectrum, we now evaluate the noise. The noise spectrum is derived by beating the fluctuations due to the laser, squeezed light and losses with the modulation sidebands.

Let us first deal with the laser fluctuations. The output laser fluctuations are

$$\delta e_{L\mathrm{out}}=\frac{r}{2}[\delta e_L(t-\tau_1)-\delta e_L(t-\tau_2)]. \tag{14}$$

In frequency space this translates into

$$\delta\tilde{e}_{L\mathrm{out}}(\omega)=ire^{i\omega\tau}\sin\left(\frac{\omega\Delta\tau}{2}\right)\delta\tilde{e}_L(\omega). \tag{15}$$

The output field $\delta e_{L\mathrm{out}}$ beats with the two modulation sidebands to give the intensity noise as

$$\delta I_L=[E^*_{b\mathrm{mod}}(\omega_L-\omega_m)e^{-i\omega_m t}+E^*_{b\mathrm{mod}}(\omega_L+\omega_m)e^{i\omega_m t}]\delta e_{L\mathrm{out}}$$
$$+[E_{b\mathrm{mod}}(\omega_L-\omega_m)e^{i\omega_m t}$$
$$+E_{b\mathrm{mod}}(\omega_L+\omega_m)e^{-i\omega_m t}]\delta e^{\dagger}{}_{L\mathrm{out}}. \tag{16}$$

From Eq. (12) we see that the modulation sidebands satisfy the following condition:

$$E^*_{b\mathrm{mod}}(\omega_L-\omega_m)=-E_{b\mathrm{mod}}(\omega_L+\omega_m),$$
$$E^*_{b\mathrm{mod}}(\omega_L+\omega_m)=-E_{b\mathrm{mod}}(\omega_L-\omega_m). \tag{17}$$

Using the above identities, in Eq. (16), we get

$$\delta I_L=E_{b\mathrm{mod}}(\omega_L+\omega_m)e^{-i\omega_m t}[\delta e^{\dagger}{}_{L\mathrm{out}}-\delta e_{L\mathrm{out}}]$$
$$+E_{b\mathrm{mod}}(\omega_L-\omega_m)e^{i\omega_m t}[\delta e^{\dagger}{}_{L\mathrm{out}}-\delta e_{L\mathrm{out}}]. \tag{18}$$

We recognize in the above equation the appearance of the output phase noise in both terms of the equation above. Using Eq. (4), this can be written as

$$\delta I_L=-iE_{b'}(\omega_L+\omega_m)e^{-i\omega_m t}X_{PL\mathrm{out}}$$
$$+-iE_{b'}(\omega_L-\omega_m)e^{i\omega_m t}X_{PL\mathrm{out}}. \tag{19}$$

In frequency space the output phase noise $\tilde{X}_{PL\mathrm{out}}(\omega)$ is related to the laser phase noise $\tilde{X}_{PL}(\omega)$ through Eq. (4) and Eq. (15),

$$\tilde{X}_{PL\mathrm{out}}(\omega)=i[\delta e^{\dagger}{}_{L\mathrm{out}}(-\omega)-\delta e_{L\mathrm{out}}(\omega)]$$
$$=ire^{i\omega\tau}\sin\frac{\omega\Delta\tau}{2}\tilde{X}_{PL}(\omega). \tag{20}$$

We now do a Fourier transform of Eq. (19) to get

$$\delta\tilde{I}_L(\omega)=re^{i(\omega-\omega_m)\tau}\sin\frac{(\omega-\omega_m)\Delta\tau}{2}$$
$$\times E_{b\mathrm{mod}}(\omega_L+\omega_m)\tilde{X}_{PL}(\omega-\omega_m)$$
$$+re^{i(\omega+\omega_m)\tau}\sin\frac{(\omega+\omega_m)\Delta\tau}{2}$$
$$\times E_{b\mathrm{mod}}(\omega_L-\omega_m)\tilde{X}_{PL}(\omega+\omega_m). \tag{21}$$

We now calculate the expectation value of the laser noise variance for frequencies around the modulation frequency, i.e., at $\omega_m+\omega_s$ to be

$$|\delta\tilde{I}_L(\omega_m+\omega_s)|^2=(r^4/4)\epsilon^2E_0{}^2\ \sin^2\left(\frac{\omega_s\Delta\tau}{2}\right)\times[|\tilde{X}_{PL}(\omega_s+2\omega_m)|^2+|\tilde{X}_{PL}(\omega_s)|^2]. \tag{22}$$

The crucial point to be noticed is that the noise measured at $\omega_m+\omega_s$ is contributed equally by the laser phase noise at frequencies ω_s and $2\omega_m+\omega_s$. The laser amplitude noise does not appear. However, if the interferometer was not of unit fringe visibility, then another term would have to be added to the total laser noise, that of the laser amplitude noise at $\omega_m+\omega_s$. The suppression factor $\sin^2\omega_s\Delta\tau/2$ (which is small for frequencies around 1 kHz) effectively reduces the phase noise contribution to the noise, especially for low frequencies.

Having evaluated the noise due to the laser we now work out in a similar way the reflected noise due to the squeezed light. The equations for the reflected squeezed fluctuations from Eq. (7) are

$$\delta e_{s\text{out}}=\frac{r}{2}[\,\delta e_s(t-\tau_1)+\delta e_s(t-\tau_2)]. \tag{23}$$

Carrying out the same calculations as we did for the laser output noise we obtain for the intensity noise due to the squeezed light,

$$|\delta\tilde{I}_S(\omega_m+\omega_s)|^2=(r^4/4)\epsilon^2E_0{}^2\ \cos^2\frac{\omega_s\Delta\tau}{2}\times[|\tilde{X}_{PS}(\omega_s+2\omega_m)|^2+|\tilde{X}_{PS}(\omega_s)|^2]. \tag{24}$$

We once again notice that the phase noise of the squeezed light determines the noise level and so if we use phase squeezed light, the total noise can be reduced below the shot noise level.

Lastly we come to the noise due to the vacuum fluctuations that leak in through the two end mirrors. The equations for the fluctuating fields $\delta e_{1,2}$, from Eq. (7) are

$$\delta e_{v1\,\text{out}}=\frac{t}{\sqrt{2}}[\,\delta e_{v1}(t-\tau_1/2)],\qquad \delta e_{v2\,\text{out}}=\frac{t}{\sqrt{2}}[\,\delta e_{v2}(t-\tau_2/2)]. \tag{25}$$

The noise due to the losses, which are contributed by each of the two arms, can be added to give

$$\begin{aligned}|\delta\tilde{I}_V(\omega_m+\omega_s)|^2&=|\delta\tilde{I}_{V1}(\omega_m+\omega_s)|^2+|\delta\tilde{I}_{V2}(\omega_m+\omega_s)|^2\\&=(\epsilon^2/4)E_0{}^2r^2t^2[|\tilde{X}_{PV1}(\omega_s+2\omega_m)|^2\\&\quad+|\tilde{X}_{PV1}(\omega_s)|^2+|\tilde{X}_{PV2}(\omega_s+2\omega_m)|^2\\&\quad+|\tilde{X}_{PV2}(\omega_s)|^2].\end{aligned} \tag{26}$$

In our model, the noise is assumed to be due to the vacuum fluctuations, for which, $|\tilde{X}_{PV1,2}(\omega)|^2=1$, for all ω. The intensity noise due to the losses then assumes a simpler form,

$$|\delta\tilde{I}_V(\omega_m+\omega_s)|^2=\frac{\epsilon^2}{2}E_0{}^2r^2t^2. \tag{27}$$

Putting together all the noise terms, the total noise is

$$\begin{aligned}&|\delta\tilde{I}_{\text{total}}(\omega_m+\omega_s)|^2\\&=\frac{\epsilon^2}{4}E_0{}^2r^4\Bigg(\cos^2\frac{\omega_s\Delta\tau}{2}[|\tilde{X}_{PS}(\omega_s+2\omega_m)|^2\\&\quad+|\tilde{X}_{PS}(\omega_s)|^2]+\sin^2\frac{\omega_s\Delta\tau}{2}[|\tilde{X}_{PL}(\omega_s+2\omega_m)|^2\\&\quad+|\tilde{X}_{PL}(\omega_s)|^2]\Bigg)+\frac{\epsilon^2}{2}E_0{}^2r^2t^2.\end{aligned} \tag{28}$$

If the laser source is QNL ($|X_{AL,PL}|^2=1$) and if the squeezed source is turned off ($|X_{AS,PS}|^2=1$), then the total noise simplifies to a simple expression,

$$|\delta\tilde{I}_{\text{total}}(\omega_m+\omega_s)|^2=\epsilon^2E_0{}^2\frac{r^2}{2}. \tag{29}$$

The noise is white when the interferometer is QNL. We can calculate the SNR $\mathcal{R}$ using the above equation as well as the equation for the strength of the signal from Eq. (13) to obtain

$$\mathcal{R}=E_0{}^2r^2(1-\epsilon^2/4)^2\frac{\phi_0{}^2}{2}\cos^2\frac{\omega_s\Delta\tau}{4}. \tag{30}$$

Frontal-phase modulation leads to the appearance of two noise terms (from different regions of the spectrum) for each source of noise. The fluctuation in intensity that one measures in an optics experiment is due to the beating of noise sidebands with a strong local oscillator. In our case we have 3 local oscillators: the carrier and the two modulation sidebands (the carrier is present only if the interferometer has an imperfect fringe visibility). Since the detection frequency is around ω_m, the carrier will bring in noise around this frequency. Whereas the modulation sidebands will bring in noise from frequencies displaced by the modulation frequency, namely, from around dc and $2\omega_m$. This was first shown in [11], where the authors considered an internally modulated interferometer. Consider the noise terms contributed by the squeezed light in Eq. (24). For small frequencies the cosine term is almost unity and therefore these two terms will dominate over the noise contributed by the laser as well as the noise due to losses (we are considering a low loss system). Hence most of the light fluctuations incident on the photodetector are due to the reflected squeezed light. We therefore see the advantage in using squeezed light as it is the major contributor of the noise and can therefore be reduced by appropriate squeezing. It is therefore necessary to use a squeezed source with squeezed phase fluctuations, with the light squeezed especially for frequencies around dc and around $2\omega_m$. However, by using squeezed light, we notice

from Eq. (28) that the total noise will become frequency dependent because the relative weights of the sine and cosine terms could now be different. This implies that the bandwidth of the interferometer will change. For a small degree of squeezing the bandwidth will not change drastically, but it is interesting to note that herein lies a potential use for squeezing. It can be used to change the bandwidth.

So far we have dealt with the simplest case of an interferometer with equal losses in the two arms. We now analyze the case when the interferometer has imperfect fringe visibility. Here we are not so much interested in calculating the SNR as much as illustrating the new features that arise in the total intensity noise. The first consequence of imperfect fringe visibility is that there will be some power distributed in the carrier that will be ejected at the output along with the modulation sidebands. This can be seen through Eq. (7) (if the reflectivities r_1 and r_2 are used). The expression for the carrier output is then

$$E_{b\,\mathrm{carr}}(\omega_L)=\tfrac{1}{2}E_0(1-\epsilon^2/4)(r_1-r_2), \tag{31}$$

where r_1, r_2 are the mirror reflectivities in the two arms. We still assume that the phase differences in the two arms are equal for the carrier frequency. The carrier now beats with the noise sidebands δe_i, where $i=1,2,3$ stand for the laser, squeezed, and vacuum (due to losses) fluctuations, respectively. From the above equation we see that the amplitude of the carrier is real and hence the intensity noise will be due to the amplitude fluctuations of the output fields, namely,

$$\delta I(t)=E_{b'}(\delta e_i+\delta e^{\dagger}_i)=E_{b'}X_{Ai}\,. \tag{32}$$

The noise variance that is due to the carrier can be calculated in a similar way as before,

$$|\delta\tilde{I}(\omega_m+\omega_s)|^2=E_0^2(1-\epsilon^2/4)^2\,\frac{(r_1-r_2)^2}{4}\left\{\left[\frac{(r_1-r_2)^2}{2}\sin^2\frac{\omega_s\Delta\tau}{2}+\frac{(r_1+r_2)^2}{2}\cos^2\frac{\omega_s\Delta\tau}{2}\right]|X_{AL}(\omega_m+\omega_s)|^2\right.$$
$$\left.+\left[\frac{(r_1-r_2)^2}{2}\cos^2\frac{\omega_s\Delta\tau}{2}+\frac{(r_1+r_2)^2}{2}\sin^2\frac{\omega_s\Delta\tau}{2}\right]|X_{AS}(\omega_m+\omega_s)|^2+(t_1^2+t_2^2)/2\right\}. \tag{33}$$

The new feature of this is that the noise contribution comes from around the modulation frequency and as explained earlier, specifically the amplitude noise of the laser as well as the squeezed source. As pointed out in [11], imperfect fringe visibility might make it imperative to have a laser source with squeezed amplitude fluctuations. For the squeezed spectrum (in addition to the squeezed phase noise at ω_s and $2\omega_m+\omega_s$), this implies that the amplitude noise at $\omega_m+\omega_s$ must be squeezed. We can estimate the strength of the noise contribution by the carrier as compared to the noise contributed by the modulation sidebands by evaluating the expression for the total noise when the laser is QNL as well as the squeezed source is turned off. Repeating the previous calculations that led to Eq. (28) (noise due to modulation sidebands) for $r_1\neq r_2$ and adding the noise term due to the carrier, Eq. (33), we get the total noise as

$$|\delta\tilde{I}_{\mathrm{total}}(\omega_m+\omega_s)|^2=E_0^2(1-\epsilon^2/4)^2\,\frac{(r_1-r_2)^2}{4}$$
$$+E_0^2\epsilon^2\frac{(r_1+r_2)^2}{8}, \tag{34}$$

where the first term is due to the carrier and the second is due to the modulation sidebands. From the above equation we can get a lower limit for the visibility below which the first term is comparable to the second. For the first term to be neglected with respect to the second, the following condition must be satisfied:

$$V\gg 1-\epsilon^2, \tag{35}$$

where V is the visibility, $V=2r_1r_2/(r_1^2+r_2^2)$. This means that for a given modulation index ($\epsilon\ll 1$), we can afford to neglect the amplitude noise at ω_m due to the laser as well as the squeezed source, provided we work with a visibility that satisfies the above criteria. For a modulation index of 0.1, the visibility must exceed 0.99. Alternatively in an experiment, if the visibility is low then the modulation index must be increased (however, the present theory has been worked out, retaining only the first-order modulation sidebands, i.e., for $\epsilon\ll 1$, so if the modulation index has to be increased considerably, then we must include higher-order sidebands) if we wanted to neglect the amplitude noise terms.

III. SIGNAL RECYCLING WITH SQUEEZED LIGHT

We now consider a signal recycled interferometer with frontal-phase modulation with the squeezed light entering the output port. In Fig. 1, the signal recycling mirror denoted by SRM is placed in front of the photodiode to recycle the gravitational-wave-induced sidebands that are generated in the arms of the interferometer. The interferometer could be in the broad-band or narrow-band mode depending on whether the signal recycling cavity (which is made up of the interferometer arms and the signal recycling mirror) is made to be resonant at the laser frequency, or at one of the gravitational-wave-induced sideband frequencies, respectively. Referring to Fig. 1, we can write down the equation for the output field in terms of the laser, squeezed, and vacuum fields as

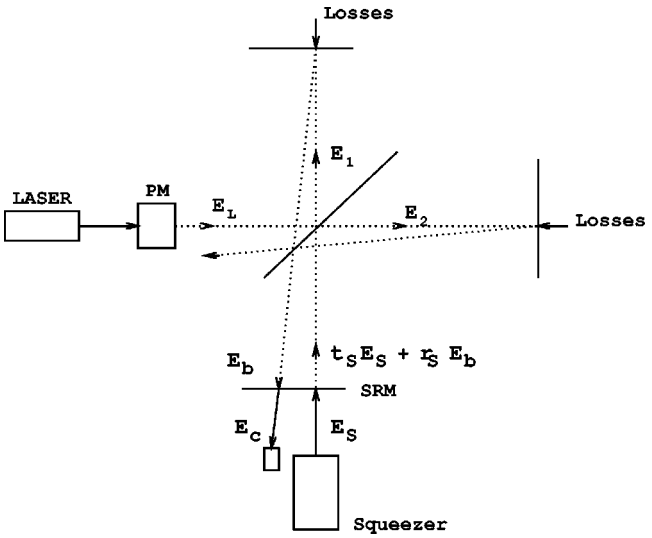

FIG. 1. The electric fields in a frontal phase modulated signal recycled interferometer. SRM, signal recycling mirror; PM, phase modulator.

$$
\begin{aligned}
E_{b'}(t) = (r/2)[&E_L(t-\tau_1-\tau_s/2)e^{i\delta\phi(t-\tau_1/2-\tau_s/2)} \\
&- E_L(t-\tau_2-\tau_s/2)e^{-i\delta\phi(t-\tau_2/2-\tau_s/2)}] \\
&+ (rt_s/2)[\delta e_s(t-\tau_1-\tau_s) + \delta e_s(t-\tau_2-\tau_s)] \\
&+ (t/\sqrt{2})[\delta e_{v1}(t-\tau_1/2-\tau_s/2) \\
&+ \delta e_{v2}(t-\tau_2/2-\tau_s/2)] + (rr_s/2)[E_{b'}(t-\tau_1-\tau_s) \\
&+ E_{b'}(t-\tau_2-\tau_s)]
\end{aligned}
$$

$$
E_c = t_s E_{b'} - r_s \delta e_s , \tag{36}
$$

where $E_{b'}(t)$ is the intracavity field, at the signal recycling mirror, E_c is the output field, which is incident on the photodiode, r_s and t_s are the signal recycling reflectivity and transitivity, and τ_s is the round trip travel time for the light, between the beam splitter and the signal recycling mirror. The recycling of light is evident from the fact that E_b' at an instant of time is related to its earlier value. We now proceed to evaluate the SNR.

In a similar way as before we get the following expressions for the gravitational-wave-induced sidebands and the modulation sidebands. They are

$$
\begin{aligned}
&E_{c\mathrm{sig}}(\omega_L \pm \omega_s) \\
&\quad = \mp \frac{t_s r}{2} \frac{E_0(1-\epsilon^2/4)e^{i\delta/2}\phi_0 \cos(\omega_s \Delta\tau/4)\, e^{\pm i\omega_s \tau/2}}{1 - r_s r e^{i\delta} e^{\pm i\omega_s \tau} \cos \omega_s \Delta\tau/2},
\end{aligned} \tag{37}
$$

$$
E_{c\mathrm{mod}}(\omega_L \pm \omega_m) = -i \frac{r t_s}{2} \epsilon E_0 e^{\pm i\omega_m \tau} e^{i\delta/2}. \tag{38}
$$

In the above equations δ is the phase offset of the signal recycling cavity from the broad-band mode and is related to τ_s by $\delta = 2\omega_L \tau_s$. This factor is adjusted by moving the signal recycling mirror and is the amount of detuning required to get the cavity off resonance from ω_L. In deriving the above equations, some of the unimportant phase factors involving τ_s have been neglected. The modulation sidebands do not get recycled if the operating point of the interferometer is at a bright fringe for them. Actually they get weakly recycled if the visibility is nonunity, but this effect can be neglected. It is convenient to define in Eq. (37) the expression for the gravitational-wave-induced sidebands, a recycling factor, $A(\omega_s)$, where

$$
A(\omega_s) = \frac{1}{1 - r_s r e^{i\delta} e^{i\omega_s \tau} \cos \omega_s \Delta\tau/2}. \tag{39}
$$

The gravitational-wave-induced sidebands beat with the modulation sidebands to give rise to the time varying intensity. In the same way as Eq. (13) was obtained, the signal spectrum at $\omega_m + \omega_s$ is

$$
\begin{aligned}
&|\delta \tilde{I}_{\mathrm{signal}}(\omega_m + \omega_s)|^2 \\
&\quad = \frac{t_s^4 r^4}{16} E_0^4 \epsilon^2 (1-\epsilon^2/4)^2 \phi_0^2 |A(\omega_s) + A^*(-\omega_s)|^2 \\
&\qquad \times \cos^2\left(\frac{\omega_s \Delta\tau}{4}\right).
\end{aligned} \tag{40}
$$

Having calculated the signal spectrum, we now evaluate the noise. We first calculate the output field fluctuations for the three noise sources (laser, squeezed, and vacuum fluctuations due to end mirror losses) in terms of $\delta e_L, \delta e_s, \delta e_{v1,2}$. Similar to Eq. (15), in frequency space, the output field fluctuations are

$$
\begin{aligned}
\delta \tilde{e}_{L\mathrm{out}}(\omega) &= i r t_s e^{i\delta/2} e^{i\omega\tau} \sin \frac{\omega \Delta\tau}{2} A(\omega)\, \delta \tilde{e}_L(\omega) \\
&= U(\omega)\, \delta \tilde{e}_L(\omega),
\end{aligned} \tag{41}
$$

$$
\begin{aligned}
\delta \tilde{e}_{s\mathrm{out}}(\omega) &= \left[r t_s^2 e^{i\delta} e^{i\omega\tau} \cos \frac{\omega \Delta\tau}{2} A(\omega) - r_s \right] \delta \tilde{e}_s(\omega) \\
&= V(\omega)\, \delta \tilde{e}_s(\omega),
\end{aligned} \tag{42}
$$

$$
\delta \tilde{e}_{V1}(\omega) = \frac{t t_s}{\sqrt{2}} e^{i\delta/2} e^{i\omega\tau_1} A(\omega)\, \delta \tilde{e}_{v1}(\omega) = W1(\omega)\, \delta \tilde{e}_{v1}(\omega), \tag{43}
$$

$$
\delta \tilde{e}_{V2}(\omega) = \frac{t t_s}{\sqrt{2}} e^{i\delta/2} e^{i\omega\tau_1} A(\omega)\, \delta \tilde{e}_{v2}(\omega) = W2(\omega)\, \delta \tilde{e}_{v2}(\omega). \tag{44}
$$

These output field fluctuations beat with the modulation sidebands to give the output intensity noise. As before, each of these noise sources contribute to the total intensity noise from two different parts of their frequency spectrum. We will restrict ourselves to the case of perfect fringe visibility and at the end of this section we will comment on the imperfect case.

The noise variance at $\omega_m + \omega_s$ for the laser noise is

$$|\delta\tilde{I}_L(\omega_m+\omega_s)|^2 = \frac{r^2t_s^2}{4}\epsilon^2E_0^2\{[|f_1|^2|X_{AL}|^2+|f_2|^2|X_{PL}|^2]_{\omega_s+2\omega_m} + [|f_1|^2|X_{AL}|^2+|f_2|^2|X_{PL}|^2]_{\omega_s}\}, \quad (45)$$

where as usual $|X_{PL}|^2, |X_{AL}|^2$ refer to the phase and amplitude noise spectra of the laser. The subscripts of the square brackets in the above equation indicate that these noise terms have to be evaluated at the frequencies, $\omega_s+2\omega_m$, and ω_s. The terms, f_1 and f_2 are

$$f_1 = 0.5\{i[U^*(-\omega)-U(\omega)]\cos\ \delta/2 - [U^*(-\omega)+U(\omega)]\sin\ \delta/2\}, \quad (46)$$

$$f_2 = 0.5i\{[U(\omega)-U^*(-\omega)]\sin\ \delta/2 + i[U^*(-\omega)+U(\omega)]\cos\ \delta/2\}.$$

In the above equations, δ is the phase offset of the signal recycling cavity from resonance with the laser light. For the broad-band case, $\delta=0$. For the narrow-band case it is adjusted such that the response of the interferometer is peaked at some desired frequency.

In a similar way, we evaluate the noise due to the squeezed light:

$$|\delta\tilde{I}_S(\omega_m+\omega_s)|^2 = r^2t_s^2\epsilon^2(E_0^2/4)\{[|g_1|^2|X_{AS}|^2+|g_2|^2|X_{PS}|^2 + 2\ \mathrm{Re}(g_1{}^*g_2)|X_{APS}|^2]_{\omega_s+2\omega_m} + [|g_1|^2|X_{AS}|^2+|g_2|^2|X_{PS}|^2 + 2\ \mathrm{Re}(g_1{}^*g_2)|X_{APS}|^2]_{\omega_s}\}, \quad (47)$$

where g_1 and g_2 are

$$g_1 = 0.5\{i[V^*(-\omega)-V(\omega)]\cos\ \delta/2 - [V^*(-\omega)+V(\omega)]\sin\ \delta/2\}, \quad (48)$$

$$g_2 = 0.5i\{[V(\omega)-V^*(-\omega)]\sin\ \delta/2 + i[V^*(-\omega)+V(\omega)]\cos\ \delta/2\}.$$

The new feature that arises with signal recycling is that the squeezed light reflects off the signal recycling cavity, to then interfere with the modulation sidebands. Hence the nature of the squeezed light that is to be sent in through the output port depends on the detuning of the cavity. This depends on whether we deal with broad-band or narrow-band signal recycling. For the broad-band case, since the cavity is at resonance with the laser light (zero detuning), the reflected squeezed light will preserve its squeezed orientation. This is because, the two correlated sidebands reflect off the cavity with exactly the opposite phase. So we would send in phase squeezed light, with the squeezing over the entire range $(0-2\omega_m)$.

In the narrow-band case, since the cavity is detuned, the two noise sidebands acquire different phase shifts and hence the squeezed orientation, changes, for different frequencies. Now, here, just as in the previous case, the squeezing should be over the whole range. However, for ease in understanding the basic problem, we will, in this case, consider broad-band squeezed light only for frequencies around dc. We therefore assume for the narrow-band case that the squeezed light is squeezed at low frequencies and is shot noise limited at high frequencies. The noise variances are taken to be

$$|X_{PS}|^2 = [\cosh 2r - \sinh 2r\cos 2\psi],$$
$$|X_{AS}|^2 = [\cosh 2r + \sinh 2r\ \cos 2\psi], \quad (49)$$
$$|X_{APS}|^2 = [\sinh 2r\ \sin 2\psi].$$

In the above equation for the phase and amplitude noise of the squeezed light, the angle ψ is an adjustable parameter that determines the angle of the squeezed ellipses, and r is the squeeze factor. We assume that the squeezed ellipses at all the frequencies start out from the squeezed source with almost the same angle. For $r>0$, and $\psi=0$, the phase noise of the squeezed light dips below the shot noise level. This reduction in noise is from Eq. (49) a factor e^{-2r}. For a reduction in the noise of 3 dB, the factor $r=0.345$. Since, for the broad-band case, we require phase-squeezed light, the angle chosen will be $\psi=0$. In the narrow-band case, we want to preadjust the angle ψ of the input squeezed light such that on reflection the reflected squeezed light comes out as phase squeezed at some frequency at which we desire to reduce the noise below the shot noise level. We also note that since squeezed light has correlations between the amplitude and phase built into them, the noise variance in Eq. (47) has a term of the form $|X_{APS}|^2$. We will make use of this when we deal with the narrow-band case.

The noise due to losses comes from both arms, hence we have two separate terms. For arm 1, the noise is

$$|\delta\tilde{I}_{V1}(\omega_m+\omega_s)|^2 = r^2t_s^2\epsilon^2(E_0^2/4)\{[|M_1|^2|X_{AV1}|^2 + |M_2|^2|X_{PV1}|^2]_{\omega_s+2\omega_m} + [|M_1|^2|X_{AV1}|^2+|M_2|^2|X_{PV1}|^2]_{\omega_s}\}, \quad (50)$$

where M_1 and M_2 are

$$M_1 = 0.5\{i[W1^*(-\omega)-W1(\omega)]\cos\ \delta/2 - [W1^*(-\omega)+W1(\omega)]\sin\ \delta/2\}, \quad (51)$$

$$M_2 = 0.5i\{[W1(\omega)-W1^*(-\omega)]\sin\ \delta/2 + i[W1^*(-\omega)+W1(\omega)]\cos\ \delta/2\}.$$

For arm 2, the noise is

$$|\delta\tilde{I}_{V2}(\omega_m+\omega_s)|^2 = r^2t_s^2\epsilon^2(E_0^2/4)\{[|N_1|^2|X_{AV2}|^2+|N_2|^2|X_{PV2}|^2]_{\omega_s+2\omega_m} + [|N_1|^2|X_{AV2}|^2+|N_2|^2|X_{PV2}|^2]_{\omega_s}\}, \quad (52)$$

where

$$N_1 = 0.5\{i[W2^*(-\omega) - W2(\omega)]\cos\,\delta/2 - [W2^*(-\omega) + W2(\omega)]\sin\,\delta/2\},$$
$$N_2 = 0.5i\{[W2(\omega) - W2^*(-\omega)]\sin\,\delta/2 + i[W2^*(-\omega) + W2(\omega)]\cos\,\delta/2\}. \quad (53)$$

The total noise then is the sum of the four terms:

$$|\delta\tilde{I}_{\rm Total}(\omega_m+\omega_s)|^2 = |\delta\tilde{I}_L(\omega_m+\omega_s)|^2 + |\delta\tilde{I}_S(\omega_m+\omega_s)|^2 + |\delta\tilde{I}_{V1}(\omega_m+\omega_s)|^2 + |\delta\tilde{I}_{V2}(\omega_m+\omega_s)|^2. \quad (54)$$

For the vacuum noise terms, the phase and amplitude noise spectra can be set to unity ($|X_{AV1,2}|^2 = |X_{PV1,2}|^2 = 1$). The signal-to-noise ratio is calculated as before, from Eq. (40) (for the signal) and the equation above for the noise, we get

$$\mathcal{R} = \frac{t_s^4 E_0^4 \epsilon^2 r^4 (1-\epsilon^2/4)^2 \phi_0^2 |A(\omega_s) + A^*(-\omega_s)|^2\, \cos^2(\omega_s \Delta\tau/4)}{16|\delta\tilde{I}_{\rm Total}(\omega_m+\omega_s)|^2}. \quad (55)$$

We now specialize to the broad-band and the narrow-band cases.

A. Broad band

In the broad-band case, the detuning $\delta = 0$. This means that the signal recycling cavity is resonant with laser light. Consider the expression for the recycling factor as defined in Eq. (39). For $\delta = 0$,

$$A(\omega_s) = \frac{1}{1 - r_s r e^{i\omega_s\tau}\cos\,\omega_s\Delta\tau/2}. \quad (56)$$

Here, for both the gravitational-wave-induced sidebands at $\omega_L \pm \omega_s$, the magnitude of the recycling factor is the same. We also notice that $A(\omega_s) = A^*(-\omega_s)$. From this we see that for the fluctuating fields as defined in Eqs. (41)–(44),

$$U(\omega) = U^*(-\omega), \quad V(\omega) = V^*(-\omega),$$
$$W1(\omega) = W1^*(-\omega), \quad W2(\omega) = W2^*(-\omega). \quad (57)$$

This physically means that the two noise sidebands equally displaced from the laser frequency resonate in a similar manner. From the expressions for $f_{1,2}, g_{1,2}, M_{1,2}, N_{1,2}$, which are defined in the equations for the intensity noise for all three noise sources and the identities defined in the previous equation, we notice that for $\delta = 0$,

$$f_1 = g_1 = M_1 = N_1 = 0. \quad (58)$$

Now, if we examine the intensity laser noise, Eq. (45), we see that $|f_1|^2$ multiplies the laser amplitude noise from frequencies around ω_s as well as $\omega_s + 2\omega_m$. This therefore implies from the previous equation that the laser amplitude noise does not appear at the output for the broad-band case. A similar reasoning shows that this is also true for the squeezed noise. Hence the total noise at the output is comprised of the phase noise terms for both the laser and squeezed source in addition to the vacuum noise due to losses. On reflection of the signal recycling cavity, the squeezed ellipses therefore do not suffer any rotation and hence the squeezed light that must be sent in should be phase squeezed. It is therefore preferable to send in phase-squeezed light, which is squeezed at frequencies all the way up to $2\omega_m$. We now define an *effective signal-to-noise ratio*, which will be used for the subsequent plots. The actual signal-to-noise ratio measured at the photodetector is what we have represented as $\mathcal{R}$. We will in all subsequent graphs plot the dimensionless quantity $\mathcal{R}_{\rm eff}$, which is defined by

$$\mathcal{R}_{\rm eff} = \mathcal{R}\frac{\hbar\omega_l}{\phi_0{}^2 P_0}, \quad (59)$$

where the power is related to $E_0{}^2$, through $P_0 = E_0{}^2\hbar\omega_l$. If we assume a measured unity signal-to-noise ratio ($\mathcal{R} = 1$), then, using the relation, $\phi_0 \simeq (h_0\omega_l\tau/2)$ [see the section before Eq. (7)] the gravitational wave amplitude will be

$$h_0^2 = \frac{1}{\mathcal{R}_{\rm eff}}\frac{\hbar c^2}{P_0\omega_l l^2}. \quad (60)$$

We use the following parameters: the average length of the arms of the interferometer are 3 km, the reflectivity of the end mirrors are $r = 0.999$, which corresponds to a loss of 2×10^{-3} in power, the modulation index, $\epsilon = 0.1$, the modulation frequency $\nu_m = 75$ MHz and the difference in the arm lengths is $\Delta L = 1$ m. For these parameters, an input power of 10 W and a power recycling factor of 100, and for a vacuum input, $h_0 = 3.3 \times 10^{-22}$. We plot in Fig. 2, $\mathcal{R}_{\rm eff}$ for the broad-band case for increasing degrees of squeezing, the signal recycling mirror reflectivity is $r_s = 0.8$. As can be seen, the SNR keeps improving as the degree of squeezing increases. As remarked earlier, the squeezed light is the major source of noise, the laser noise being heavily suppressed. In any realistic squeezed source, we would not expect broad-band squeezing over such a large range of frequencies. This means that whatever the spectrum of squeezing that we get out of the squeezer, it should be phase squeezed light at least at low frequencies up to 1 kHz and once again the same feature repeated at $2\omega_m$.

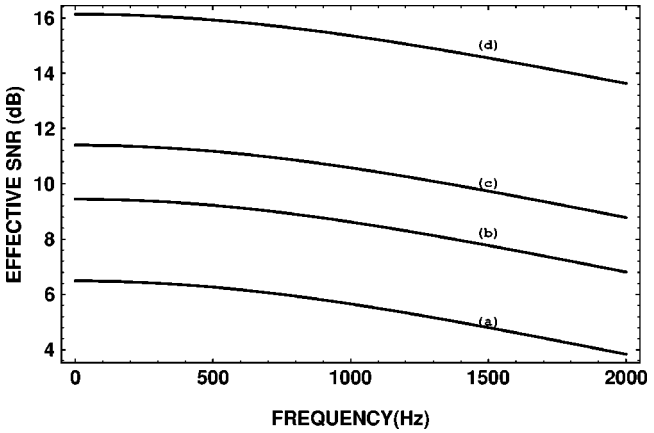

FIG. 2. The broad-band curves for different amounts of squeezing. Curves (a), (b), (c), and (d) are for a vacuum input, 3, 5, and 10 dB squeezing, respectively.

B. Narrow band

In the narrow-band case, the detuning is adjusted so that the signal recycling cavity is resonant at one of the gravitationally induced sidebands. The signal power in this sideband is enhanced by the recycling mirror SRM. The other sideband is out of phase with the cavity and its amplitude is considerably diminished. As the signal recycling reflectivity is increased, the signal cavity is effectively made up of mirrors with almost equal reflectivity and the maximum signal power is stored. From Eq. (39), we see that the recycling factor $A(\omega_s)$ (which is responsible for the enhancement in the sideband power at the frequency $\omega_L+\omega_s$) can be enhanced for a certain frequency ω_{s0}, if the following condition is satisfied,

$$\delta=-\omega_{s0}\tau. \tag{61}$$

The recycling factor then becomes

$$A(\omega_s)=\frac{1}{1-r_s r e^{i(\omega_s-\omega_{s0})\tau}\cos\,\omega_s\Delta\tau/2}. \tag{62}$$

For frequencies within 1 KHz and for $\Delta\tau=1$ m, the cosine factor is almost unity. Hence, for a very highly reflecting signal recycling mirror, $|A(\omega_s)|$ can be very large and peaks at $\omega_s=\omega_{s0}$. From Eq. (62), expanding the exponential for frequencies around ω_{s0}, we get

$$|A(\omega_s)|^2\simeq\left[\frac{1}{(1-r_s r)^2}\right]\left[\frac{1}{1+(\omega_s-\omega_{s0})^2/\delta\omega_B^2}\right]. \tag{63}$$

The above function is a Lorenzian, strongly peaked about ω_{s0} with a bandwidth,

$$\delta\omega_B=\frac{1-r_s r}{r_s r\tau}. \tag{64}$$

As r_s approaches unity, the recycling factor gets larger and more narrow. Thus one of the signal sidebands is considerably enhanced. The recycling factor for the other sideband is

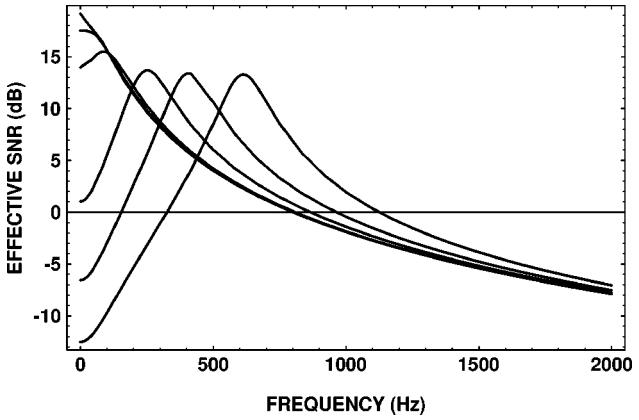

FIG. 3. The graph shows how the effect of increasing amounts of detuning makes the response narrower. The various curves shown are for the detuning, $\delta=0$, 5, 10, 30, 50, and 76 mrad.

$$A(\omega_{s0})\simeq\frac{1}{1-r_s r e^{-2i(\omega_{s0})\tau}}. \tag{65}$$

We can see that the other sideband gets relatively suppressed because of the phase factor. In Fig. 3 we plot the $\mathcal{R}_{\rm eff}$ for the broad-band case for all the sources shot noise limited and then slowly vary the detuning parameter. We see the slow transition from the broad-band to the narrow-band regime. The $\mathcal{R}_{\rm eff}$ gradually develops a peak at a higher frequency, where the sensitivity is much larger than that for the broad-band case. The curves have been obtained for $r=0.999$, $r_s=0.99$, and $\delta=0$, 5, 10, 30, 50, and 76 mrad. At $\delta=76$ mrad, the $\mathcal{R}_{\rm eff}$ peaks at 600 Hz. The peak of the sensitivity drops below that of the low-frequency sensitivity of the broad band by a factor of around 6 dB. This is because only one of the sidebands gets recycled.

The bandwidth $\delta\omega_B$ in Eq. (64) is not the real bandwidth of the interferometer since in deriving this expression, we have not taken into account the noise. If all the noise sources are QNL and the squeezed source is turned off then it will be the bandwidth. This is because the total noise at the output will be white noise. However, as mentioned above this will not be true once squeezed light is injected.

When squeezed light is injected into the output port, it gets reflected from the signal recycling cavity. Since the cavity is not resonant at the laser frequency and is detuned, the two noise sidebands acquire different phase shifts. As a result the squeezed ellipses get rotated at different angles, relative to each other, when they emerge after reflection. The angle ψ, the squeeze angle, is adjusted so as to minimize the squeezed noise in Eq. (47) at the frequency ω_{s0}. This means that ψ is chosen in such a way that after reflection the noise ellipse at ω_{s0} comes out as phase squeezed. In Fig. 4 we plot the $\mathcal{R}_{\rm eff}$ for an input of 10-dB squeezing [curve (b)] and compare it to the vacuum input case [curve (a)] (for the same parameters as in Fig. 3). The improvement in sensitivity at the resonant frequency (600 Hz) compared to the shot noise curve (vacuum input) has increased with the squeezing. However, the improvement does not seem to be substantial, it is an improvement of only about 2 dB. However, we must recollect that we have considered squeezing only at low frequencies, whereas in the total noise, there is another term at

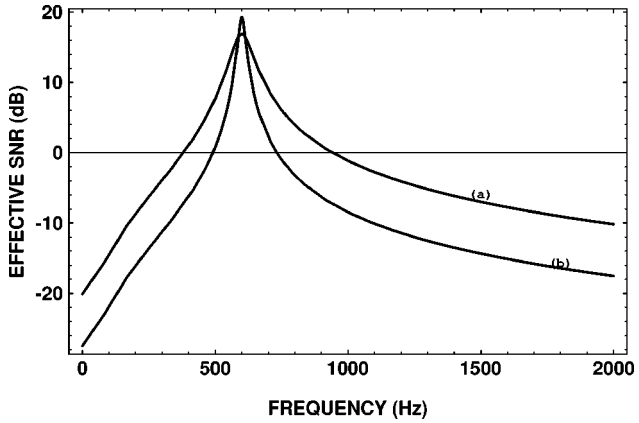

FIG. 4. The narrow-band curves for a vacuum input and 10-dB squeezing. Curves (a) and (b) are for vacuum and 10 dB, respectively.

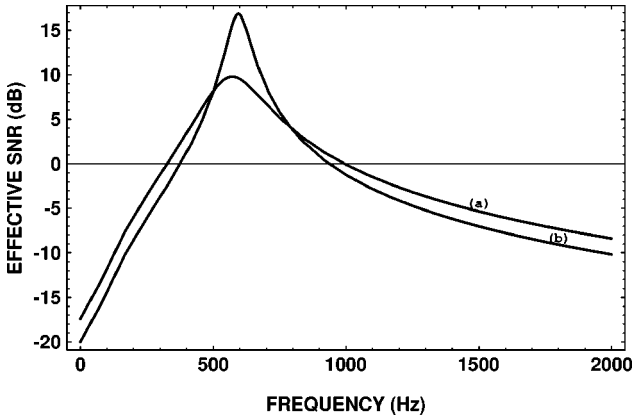

FIG. 5. The narrow-band curves for a vacuum input and 10 dB squeezing, with the noise reduction at 100 Hz. Curves (a) and (b) are for 10 dB squeezing and vacuum input, respectively.

$2\omega_m+\omega_s$ that we had for simplicity assumed to be QNL. Hence if the squeezed spectrum is extended all the way up to twice the modulation frequency, we can expect substantial improvement in the sensitivity. However, here we deal only with low-frequency squeezing to bring out the essential points.

We also notice that the bandwidth decreases. This is because, for the resonant frequency ω_{s0} (600 Hz), the squeezed noise ellipse comes out phase squeezed and this reduces the noise at this frequency thus increasing the SNR. However, the noise ellipses at the other frequencies around ω_{s0} acquire a relative rotation and hence they do not come out as phase squeezed. Therefore the noise at the wings gets worse and this is why the SNR drops more rapidly in comparison to the shot noise case. However, this happens in our model because we had chosen to send in the noise ellipses at the same angle, this being the simplistic case. If it were possible to engineer the squeezed light such that the ellipses go in at different angles, but each angle is chosen such that on reflection it comes out as phase squeezed, then the SNR would increase in the wings as well and thus the whole curve would shift upwards. This is in fact the case considered in [10], where squeezed light was used in a dual recycled interferometer. In this case, the sensitivity at all frequencies increases and thus the bandwidth remains unaffected.

Let us consider the case when the noise reduction is made not at ω_{s0} but at some other frequency $\omega_{s'}$. We could do this by adjusting the squeeze angle ψ such that when the noise ellipses come back reflected, the noise ellipse at $\omega_{s'}$ is phase squeezed. As we move away from this frequency (towards ω_{s0}), the noise ellipses change their orientation and the reflected noise gets worse. On the other side of ω_{s0}, at some frequency, the ellipses have rotated by π and here once again there is a noise reduction. So we expect that the SNR starts out being better than that of the vacuum input at $\omega_{s'}$, gets progressively worse as we approach ω_{s0}, and then starts to improve once again as we go further out. This is the reason we would expect an increased bandwidth at the loss of some SNR at ω_{s0}. This can be seen in Fig. 5 where we plot the SNR for 10 dB of squeezing [curve (a)] (with the same parameters as was used for Fig. 4) comparing it to the vacuum input [curve (b)]. The squeezed noise in this case has been minimized at a frequency of 100 Hz by suitably adjusting the squeeze angle. Here we notice that in addition to the increased bandwidth, the peak of the SNR has shifted by a small amount. Our choice of ψ that minimizes the noise at $\omega_{s'}$ and not at ω_{s0} means that we will find some intermediate frequency between ω_{s0} and $\omega_{s'}$ at which, although the signal here is weaker than at ω_{s0}, the noise, however, is lower than at ω_{s0}, thus maximizing the SNR. This implies that by changing the squeezed angle (which naturally minimizes the noise at some frequency), we can shift the peak by a small amount although reducing the sensitivity at the new peak. This therefore simulates the detuning of the cavity, which might have to be done with a servo. This might find use in trying to search for a continuous wave source, the frequency of which is uncertain by a small amount. In Fig. 6, the SNR for the vacuum input [curve (b)] is compared to that of 10 dB of squeezing [curve (a)] but with a slight difference. The signal cavity is purposely detuned by a small amount so that the shift in the peak of the SNR for 10 dB of squeezing can sit at the resonant frequency which for us is at 600 Hz. We can clearly see the increase in the bandwidth for the 10-dB curve.

It is interesting to see what happens when the signal mirror reflectivity is chosen to be equal to the reflectivity of the

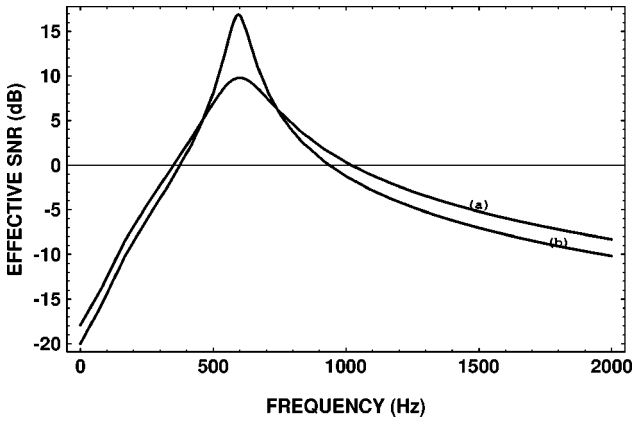

FIG. 6. The narrow-band curves for a vacuum input and 10-dB squeezing with the noise reduction at 100 Hz, after detuning the cavity to bring back the peak of the SNR back to the resonant frequency. Curves (a) and (b) are for 10 dB squeezing and vacuum input, respectively.

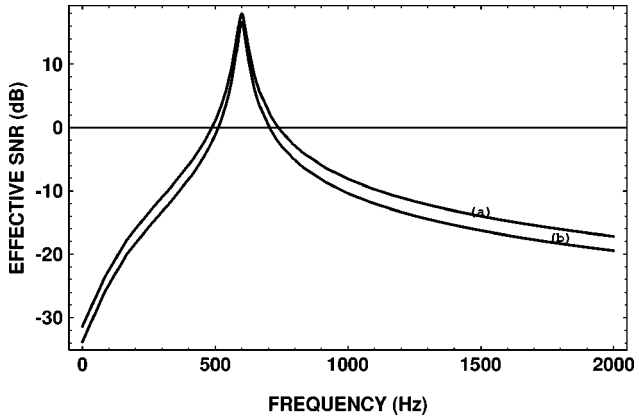

FIG. 7. The narrow-band curves for a vacuum input and 10-dB squeezing, for the impedence matched case, with noise reduction at the resonant frequency. Curves (a) and (b) are for a vacuum input and 10-dB squeezing, respectively.

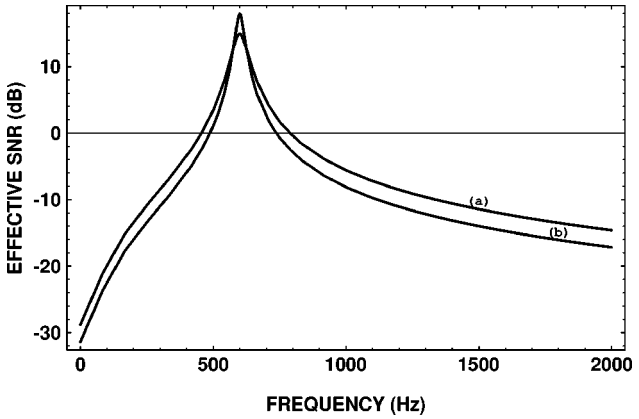

FIG. 8. The narrow-band curves for a vacuum input and 10-dB squeezing for the impedence matched case with the noise reduction at 100 Hz. Curves (a) and (b) are for 10-dB and a vacuum input, respectively.

end mirrors. This case is like impedence matching, since we now have the signal recycling cavity resonant at ω_{s0}, with equal reflectivity mirrors and this corresponds to the case when a maximum buildup in signal power is possible. Figure 7 shows the $\mathcal{R}_{\rm eff}$ for the impedence matched case comparing the vacuum input [curve (a)] with an input of 10 dB of squeezing [curve (b)] with $r=r_s=0.999$. At ω_{s0}, there is no improvement in the SNR. In fact it gets slightly worse for the 10-dB curve. To understand the reason the noise at ω_{s0} gets worse, let us consider in detail the reflection of squeezed light off a cavity. Consider a cavity with identical reflecting mirrors, of reflectivity r and round trip travel time τ and a detuning δ of the cavity from resonance with laser light. Then the reflectivity is

$$R(\omega)=\frac{-r(1-e^{i(\omega\tau+\delta)})}{1-r^2e^{i(\omega\tau+\delta)}}. \tag{66}$$

Consider squeezed light $\delta E_s(\omega)$ that is reflected off this cavity. We measure the phase quadrature of the reflected light, $\delta E_{\rm out}(\omega)$. The output phase quadrature will be made up of the reflected squeezed light and the transmitted noise sidebands, which are due to losses. For the squeezed light component of the reflected light, we get

$$\begin{aligned}X_{P\rm out}(\omega)&=i[\,\delta E^{\dagger}_{\rm out}(-\omega)-\delta E_{\rm out}(\omega)\,]\\&=i[R^*(-\omega)\,\delta E^{\dagger}_s(-\omega)-R(\omega)\,\delta E_s(\omega)].\end{aligned} \tag{67}$$

In terms of the phase and amplitude quadratures of the input light, the above equation can be written as

$$\begin{aligned}X_{P\rm out}(\omega)=&\frac{i}{2}[R(\omega)-R^*(-\omega)]X_{As}(\omega)\\&-\tfrac{1}{2}\,[R^*(-\omega)+R(\omega)]X_{Ps}(\omega).\end{aligned} \tag{68}$$

Consider the detuning to be such that the cavity is resonant at ω_0. Then, $\delta=-\omega_0\tau$. From Eq. (66) we see that the reflectivity is zero. The reflected squeezed noise at ω_0 is due to the correlation of the two noise sidebands at $\omega_L\pm\omega_0$. One of these sidebands is transmitted through the cavity [since $R(\omega_0)=0$], whereas the other is partially reflected. Substituting in Eq. (68), for $R(\omega_0)=0$, we see that the phase quadrature at the output (at ω_0) is

$$\begin{aligned}X_{P\rm out}(\omega_0)=&\frac{-i}{2}[R^*(-\omega_0)]X_{As}(\omega_0)\\&+\frac{1}{2}[R^*(-\omega_0)]X_{Ps}(\omega_0).\end{aligned} \tag{69}$$

Notice that the two quadratures come back after reflection with equal contributions but are out of phase by $\pi/2$. The noise spectrum can be calculated to be [in the same way as Eq. (47)]

$$|X_{P\rm out}(\omega_0)|^2=\tfrac{1}{2}\,|R(-\omega_0)|^2\,\cosh(2r). \tag{70}$$

The noise ellipse at ω_0, after reflection, comes out rotated to increase the noise by a factor $\cosh(2r)$ as compared with the vacuum input case. This explains why the 10-dB curve for the narrow band case is slightly worse in SNR as compared to the vacuum input at $\omega_{s0}=600$ Hz. The bandwidth for the 10-dB case, as can be seen in Fig. 7 decreases for the same reason as mentioned in the previous paragraphs.

In Fig. 8 the noise reduction is made at some other frequency, for example, 100 Hz. We notice that the SNR gets broader for the 10-dB squeezing case [curve (a)] as compared to the vacuum input [curve (b)]. However, the peak sensitivity for the curve with squeezing decreases by a lesser amount than the nonimpedence matched case at ω_{s0}. For the impedence matched case, the signal drops very rapidly for frequencies around ω_{s0} and hence the shift of the SNR peak in this case is not significant. If we compare the bandwidth of all the three cases (vacuum input and noise reduction at 600 and 100 Hz) then the bandwidth (which we define as full

width at half maximum) turns out to be 100.05 Hz for the vacuum input, 89.3 Hz for the 10-dB squeezed light (with the noise reduction at $\omega_0 = 600$ Hz), and 190.5 Hz (with the noise reduction at 100 Hz). The bandwidth can therefore be changed considerably by manipulating the squeezed angle without too much of a loss in sensitivity at the resonant frequency. From this we could expect to use the squeezed light as a bandwidth modulator, that is, by changing the squeeze angle and hence changing the frequency at which the noise is reduced, we could fine tune the bandwidth.

We finally consider the case of imperfect fringe visibility. If the losses in the two arms are unequal then some of the carrier leaks through. Along with the carrier come the amplitude and phase fluctuations of the three noise sources at $\omega_m + \omega_s$. For the broad-band case it is only the amplitude fluctuations that leak through. Hence, with imperfect fringe visibility, the amplitude spectrum of the laser and squeezed light source must dip below the shot noise for frequencies around ω_m. In the case of the narrow band, because of the detuning, a small amount of phase fluctuations at $\omega_m + \omega_s$ leak through (in addition to the amplitude fluctuations). To get a quantitative measure of how important imperfect fringe visibility is we must compare the noise terms that come in because of the carrier with the noise terms that are present due to the modulation sidebands. The new noise terms have been displayed in the Appendix. A comparison of these terms for a QNL laser and vacuum input in the broad-band case shows that for the carrier noise terms to be neglected versus the modulation noise terms, the following condition must be met:

$$V \geqslant \frac{2 - \epsilon^2 - \epsilon^2/F}{2 - \epsilon^2 + \epsilon^2/F}, \tag{71}$$

where $F = 1/(1 - r_s r)^2$. For r_s very close to unity, F could be very large. Hence from the above equation, it is clear that the visibility will have to be very good for the carrier noise terms to be neglected. The demands placed on the visibility are more stringent here than in the nonrecycled case because the power in the carrier increases due to recycling. The intensity noise due to the carrier therefore increases. For $r_s = 0.99$ and $r = 0.999 (r = (r_1 + r_2)/2)$, $F \simeq 10^4$. If the modulation index is 0.1 then this implies that the visibility must be greater than $1 - 10^{-6}$. It is questionable whether this value of V can be achieved for the currently planned high power laser interferometers. There are other effects such as thermal lensing and birefringence that will seriously limit the visibility to a much smaller value.

IV. CONCLUSIONS

In this paper we analyzed a frontal-phase-modulated signal recycled interferometer with squeezed light (vacuum) injected through the signal recycling mirror. We analyzed the SNR using a linearized theory of treating quantum noise. This technique brings out the origin of the different contributions to the noise spectra and their relative contributions to the total noise. With this technique we can generate expressions for the total output noise that allow us to use experimentally generated input noise spectra.

We first developed a model of a frontal-modulated simple Michelson interferometer with a squeezed input. The results we obtained for a simple Michelson interferometer, not surprisingly, are similar to results that were first obtained for the internally modulated case [11]. We found that the squeezed input field needs to be phase squeezed at low frequencies and for frequencies around twice the modulation frequency to make a significant improvement in the sensitivity. We analyzed the case when the losses in the two arms are unequal. As a result of this, additional noise terms are coupled in to the detector. This sets stringent requirements on the visibility for these terms to be negligible or requires more complex squeezing spectra (for example, in addition to phase squeezing we must also use amplitude squeezed light at the modulation frequency).

We then considered signal recycling. The required spectrum of squeezing for broad-band signal recycling remains essentially the same as for a simple Michelson interferometer. However, this is not true for the narrow-band case. Narrow-band interferometers, in general, require more complex squeezed spectra (once again squeezed for low frequencies and for frequencies around $2\omega_m$) for substantial improvements in the SNR. We found that if we use broad-band squeezing injected into an overcoupled cavity, then a substantial improvement in sensitivity can be achieved at the resonant frequency of the signal cavity, at the cost of a reduced bandwidth for the interferometer. We found that the frequency of peak response could be altered by changing the input spectrum of the squeezed light. Thus squeezed light could be used to tune the resonant frequency of the cavity without actually moving the signal recycling mirror. In the impedence matched case we found that squeezing does not increase the sensitivity at the resonant frequency. However, squeezing could be used to change the bandwidth of the interferometer without substantially decreasing the sensitivity at the resonant frequency. Though complex, it should be possible to produce the required squeezing spectra, for example by reflecting squeezed light from a parametric amplifier off a suitably chosen cavity system [14].

An important point to note is that the frontal modulation, signal recycling scheme examined here can be extended to produce all the necessary information to control a dual recycled interferometer [15]. However, it cannot generate an efficient signal extraction scheme in the case of a tuned dual recycling. In this case, for signal extraction, an external modulation scheme can be employed. As many of the results presented here are generic to phase modulation, we anticipate them to be applicable with modification to a full dual recycling interferometer incorporating both frontal and external modulation.

ACKNOWLEDGMENTS

V.C. would like to express gratitude to Professor R. J. Sandeman as well as several members of the Quantum Optics group at the Australian National University, Canberra, where this research was carried out. He would also like to acknowledge Professor J. V. Narlikar, the UGC, and COSTED for their generous support.

APPENDIX

In the Appendix we give expressions for the total noise when we have to deal with imperfect fringe visibility. The new terms that appear are those associated with the carrier. As discussed in Sec. II, the noise that comes in with the carrier for the three noise sources contributes noise from frequencies around the modulation frequency in their spectra. With signal recycling for imperfect fringe visibility the expressions for the carrier and the modulation sidebands are

$$E_{c'}(\omega_L)=\frac{t_s E_0(1-\epsilon^2/4)e^{i\delta/2}(r_1-r_2)}{2(1-r_s(r_1+r_2)e^{i\delta}/2)}=E_{c'}=|E_{c'}|e^{i\chi}, \tag{A1}$$

$$E_{c'}(\omega_L\pm\omega_m)=E_{b'}(\omega_L\pm\omega_m)=\frac{-it_s(r_1+r_2)}{4}\epsilon E_0 e^{\pm i\omega_m\tau}. \tag{A2}$$

Similar to Eqs. (41)–(44), the expressions for the output fluctuations for the three sources are

$$\delta\tilde{e}_{L\text{out}}(\omega)=t_s e^{i\delta/2}e^{i\omega\tau}\left[i(r_1+r_2)\sin\frac{\omega\Delta\tau}{2}+(r_1-r_2)\cos\frac{\omega\Delta\tau}{2}\right]A(\omega)\delta\tilde{e}_L(\omega)=U(\omega)\delta\tilde{e}_L(\omega), \tag{A3}$$

$$\delta\tilde{e}_{s\text{out}}(\omega)=\frac{t_s^2}{2}e^{i\delta}e^{i\omega\tau}\left[(r_1+r_2)\cos\frac{\omega\Delta\tau}{2}+i(r_1-r_2)\sin\frac{\omega\Delta\tau}{2}\right][A(\omega)-r_s]\delta\tilde{e}_s(\omega)=V(\omega)\delta\tilde{e}_s(\omega), \tag{A4}$$

$$\delta\tilde{e}_{V1}(\omega)=\frac{t_1 t_s}{\sqrt{2}}e^{i\delta/2}e^{i\omega\tau_1}A(\omega)\delta\tilde{e}_{v1}(\omega)=W1(\omega)\delta\tilde{e}_{v1}(\omega), \tag{A5}$$

$$\delta\tilde{e}_{V2}(\omega)=\frac{t_2 t_s}{\sqrt{2}}e^{i\delta/2}e^{i\omega\tau_1}A(\omega)\delta\tilde{e}_{v2}(\omega)=W2(\omega)\delta\tilde{e}_{v2}(\omega). \tag{A6}$$

The noise variances (with the same definitions as before) are

$$|\delta\tilde{I}_L(\omega_m+\omega_s)|^2=|E_{c'}(\omega_L)|^2[|f_1|^2|X_{AL}|^2+|f_2|^2|X_{PL}|^2]_{\omega_s+\omega_m}+|E_{c'}(\omega_L+\omega_m)|^2\{[|f_1|^2|X_{AL}|^2+|f_2|^2|X_{PL}|^2]_{\omega_s+2\omega_m}$$
$$+[|f_1|^2|X_{AL}|^2+|f_2|^2|X_{PL}|^2]_{\omega_s}\}, \tag{A7}$$

$$|\delta\tilde{I}_S(\omega_m+\omega_s)|^2=|E_{c'}(\omega_L)|^2[|g_1|^2|X_{AS}|^2+|g_2|^2|X_{PS}|^2]_{\omega_s+\omega_m}+|E_{c'}(\omega_L+\omega_m)|^2\{[|g_1|^2|X_{AS}|^2+|g_2|^2|X_{PS}|^2]_{\omega_s+2\omega_m}$$
$$+[|g_1|^2|X_{AS}|^2+|g_2|^2|X_{PS}|^2+2\,\mathrm{Re}(g_1^* g_2)|X_{APS}|^2]_{\omega_s}\}, \tag{A8}$$

$$|\delta\tilde{I}_{V1}(\omega_m+\omega_s)|^2=|E_{c'}(\omega_L)|^2[|M_1|^2|X_{AV1}|^2+|M_2|^2|X_{PV1}|^2]_{\omega_s+\omega_m}+|E_{c'}(\omega_L+\omega_m)|^2\{[|M_1|^2|X_{AV1}|^2$$
$$+|M_2|^2|X_{PV1}|^2]_{\omega_s+2\omega_m}+[|M_1|^2|X_{AV1}|^2+|M_2|^2|X_{PV1}|^2]_{\omega_s}\}, \tag{A9}$$

$$|\delta\tilde{I}_{V2}(\omega_m+\omega_s)|^2=|E_{c'}(\omega_L)|^2[|N_1|^2|X_{AV2}|^2+|N_2|^2|X_{PV2}|^2]_{\omega_s+\omega_m}+|E_{c'}(\omega_L+\omega_m)|^2\{[|N_1|^2|X_{AV2}|^2+|N_2|^2|X_{PV2}|^2]_{\omega_s+2\omega_m}$$
$$+[|N_1|^2|X_{AV2}|^2+|N_2|^2|X_{PV2}|^2]_{\omega_s}\}. \tag{A10}$$

For each $|\delta\tilde{I}(\omega_m+\omega_s)|^2$ displayed above, the first term represents the noise fluctuations that enter with the carrier and the second and third terms are due to the modulation sidebands. In all of the above equations the definitions of f_1, f_2, etc. are the same as those in Eq. (46), (48), (51), (53). The total noise is

$$|\delta\tilde{I}_{\text{total}}(\omega_m+\omega_s)|^2=|\delta\tilde{I}_L(\omega_m+\omega_s)|^2+|\delta\tilde{I}_S(\omega_m+\omega_s)|^2+|\delta\tilde{I}_{V1}(\omega_m+\omega_s)|^2+|\delta\tilde{I}_{V2}(\omega_m+\omega_s)|^2. \tag{A11}$$

[1] K. S. Thorne, in *300 Years of Gravitation*, edited by S. W. Hawking and W. Israel (Cambridge University Press, Cambridge, 1987).

[2] A. Giazotto *et al.*, Phys. Rep. **182**, 365 (1989).

[3] Andrew J. Stevenson *et al.*, Appl. Opt. **32**, 3481 (1993).

[4] Malcolm Gray *et al.*, Appl. Opt. **35**, 1623 (1996).

[5] L. Schnupp (unpublished).

[6] C. M. Caves, Phys. Rev. D **23**, 1693 (1981); for an overview see, D. F. Walls and G. J. Milburn, *Quantum Optics* (Springer-Verlag, Berlin, 1994).

[7] R. W. P. Drever, in *Gravitational Radiation*, edited by N. Deruelle and T. Piran (North-Holland, Amsterdam, 1983); J. Y. Vinet, B. J. Meers, C. N. Man, and A. Brillet, Phys. Rev. D **38**, 433 (1988).

[8] B. J. Meers, Phys. Rev. D **38**, 2317 (1988); B. J. Meers, Phys. Lett. **14A**, 465 (1989); K. A. Strain and B. J. Meers, Phys. Rev. Lett. **66**, 1391 (1991); A. Krolak, J. A. Lobo, and B. J. Meers, Phys. Rev. D **43**, 2470 (1991).

[9] A. Brillet, J. Gea-Banacloche, G. Leuchs, C. N. Man, and J. Y. Vinet, in, *The Detection of Gravitational Radiation*, edited by D. Blair (Cambridge University Press, Cambridge, 1991).

[10] Vijay Chickarmane and S. V. Dhurandhar, Phys. Rev. A **54**, 786 (1996).

[11] J. Gea Banacloche and G. Leuchs, J. Opt. Soc. Am. B **4**, 1667 (1987); J. Mod. Opt. **34**, 793 (1987).

[12] M. T. Jaekel and S. Reynaud, Europhys. Lett. **13**, 301 (1990); S. Reynaud *et al.*, in *Progress in Optics*, edited by E. Wolf (North-Holland, Amsterdam, 1992), Vol. XXX, p. 3; see the lectures by C. Fabre and S. Reynaud, in *Fundamental Systems in Quantum Optics*, Les Houches Summer School Session LIII, edited by J. Dalibard, J.-M. Raimond, and J. Jinn-Justin (North-Holland, Amsterdam, 1992), p. 675.

[13] For a review see, Andrew J. Stevenson *et al.*, Aust. J. Phys. **48**, 971 (1995); see also P. Saulson, *The Detection of Gravitational Waves* (World Scientific, Singapore, 1996).

[14] P. Galatola *et al.*, Opt. Commun. **85**, 95 (1991).

[15] Malcolm Gray *et al.* (unpublished).